CHAPTER 11

Strategies for Building Protein–Glycosaminoglycan Interaction Networks Combining SPRi, SPR, and BLI

SYLVAIN D. VALLET,[a] LISETTE DEDDENS,[b] ARNAUD VONARBURG,[b] ROMAIN SALZA,[a,†] CLÉMENT FAYE,[a,‡] ATTILA ARANYOS,[b] NICOLAS THIERRY-MIEG[c] AND SYLVIE RICARD-BLUM*[a]

[a] Institut de Chimie et Biochimie Moléculaires et Supramoléculaires, UMR 5246 CNRS – Université Lyon 1, 69622 Villeurbanne, France; [b] Pall FortéBio; [c] TIMC-IMAG, UMR 5525 CNRS – Université Grenoble Alpes, La Tronche, France
*Email: sylvie.ricard-blum@univ-lyon1.fr

11.1 Introduction

The extracellular matrix (ECM) is a structural scaffold contributing to the organization and mechanical properties of tissues[1,2] and is a key player in tissue failure.[3] The ECM modulates cell behavior *via* several receptors and

[†]Present address: Histalim, Montpellier, France.
[‡]Present address: Colcom, Clapiers, France.

Handbook of Surface Plasmon Resonance, 2nd Edition
Edited by Richard B. M. Schasfoort
© The Royal Society of Chemistry 2017
Published by the Royal Society of Chemistry, www.rsc.org

this dynamic structure constantly undergoes remodeling,[4] which leads to diseases if uncontrolled.[5] Understanding these mechanisms is essential for finding novel therapeutic targets and designing strategies for regenerative medicine.[4,6] ECM molecules are therefore important targets for pharmacotherapy.[7] The structure and functions of the intricate 3D ECM network rely on numerous interactions, and the identification of key interactions for ECM assembly and cell interplay is a prerequisite to determining how they are disturbed in diseases.

The human ECM is comprised of 274 proteins forming the core matrisome (*e.g.* collagens, laminins, fibronectin, elastin, and proteoglycans) and of 747 matrisome-associated proteins, which are secreted factors, ECM regulators (degradation and crosslinking enzymes), and ECM-affiliated proteins (*e.g.* semaphorins, galectins, mucins).[8,9] The ECM is a source of bioactive fragments (matricryptins), which are released from extracellular proteins by proteolysis, and have biological activities of their own.[10–12] Endostatin, a C-terminal proteolytic fragment of collagen XVIII, is one of the most studied matricryptins. It is both anti-angiogenic and anti-tumoral,[10,13] has ATPase activities,[14] and contributes to host–pathogen interactions.[15] In addition to proteins, the ECM contains five sulfated glycosaminoglycans (GAGs), chondroitin sulfate, dermatan sulfate, keratan sulfate, heparin, and heparan sulfate, which are covalently linked to proteins to form proteoglycans,[16] and hyaluronan, a non-sulfated GAG.

GAGs are complex, linear polysaccharides made of repeating disaccharide units comprising a hexuronic acid (or a galactose for keratan sulfate) and a hexosamine. Heparin (HP) and heparan sulfate (HS) share the same disaccharide unit and are extensively modified by several enzymes during and after their synthesis.[17] They both have tremendous structural diversity and 23 HS disaccharides have been identified *in vivo*[18] out of the 48 theoretically possible HS disaccharides.[19] Heparan sulfate is less sulfated than heparin and is organized into highly sulfated domains and *N*-acetylated domains interspersed with domains of intermediate sulfation. Heparin and heparan sulfate interact with at least 435 proteins,[20,21] including ECM proteins, growth factors, chemokines, enzymes, and receptors such as integrins.[22] These interactions are involved in numerous biological processes such as development, angiogenesis, tumor growth, host–pathogen interactions, inflammation, ECM assembly, cell–matrix interactions, and signaling. The identification of the sulfate groups involved in protein recognition, the determination of the minimal size of heparin required for binding to its partners, and the calculation of their association rate to, and dissociation rate from, their partners together with the affinity are required to decipher the molecular mechanisms underlying their biological roles at the individual level.[22] However the building of GAG–protein interaction networks is required to determine how these individual interactions influence each other *in vivo*, form networks in various biological processes, and are altered in diseases.

11.2 A Roadmap to Build Protein–Glycosaminoglycan Interaction Networks

Protein–GAG interaction networks are built from experimental data and from manual curation of the literature. The interaction database developed in our laboratory, MatrixDB[23–25] (http://matrixdb.univ-lyon1.fr), focuses on interactions involving at least one extracellular matrix protein or GAGs and is one of the very few databases, if any, reporting protein–GAG interactions and thus giving the possibility for users to build not only protein–protein interaction networks but also GAG–protein interactomes as described below. MatrixDB belongs to the International Molecular Exchange consortium (www.imexconsortium.org), and follows the consortium curation rules to report interaction data.[26] We perform literature curation through the interface developed by another interaction database, IntAct[27] (www.ebi.ac.uk/intact). Interaction data curated by MatrixDB and the other IMEx consortium databases are freely available and can be downloaded from their websites. We have developed a roadmap comprising the following steps to build and analyze protein–protein and protein–GAG interaction networks:

1. Identification of biomolecular interactions by screening about 100 potential interactors spotted in triplicate onto a gold surface by surface plasmon resonance imaging (SPRi) in a Biacore Flexchip system (GE Healthcare). This instrument is based on grating-coupled SPR sensor chips consisting of a plastic optical grating coated with a thin (~80 nm) layer of gold onto which biomolecules are spotted[28] and is described in Section 11.3.
2. Calculation of kinetic parameters (association and dissociation rates) and equilibrium dissociation constant (K_D) by SPR (Biacore T100/T200, GE Healthcare) and/or Bio-Layer Interferometry (BLI) (Octet RED96, Pall FortéBio). These parameters are used to prioritize interactions within a network and to evaluate the half-lives of the interactions.[22] Binding sites are either identified experimentally through site-directed mutagenesis and binding assays performed with mutants or predicted *in silico* by molecular modeling when possible.
3. Visualization of the interaction networks either with MatrixDB iNavigator[25] (http://matrixdb.univ-lyon1.fr) or with Cytoscape (www.cytoscape.org), an open-source software platform,[29] which is also used to calculate the metrics of the networks (*e.g.* shortest path, diameter, betweenness) and to contextualize the networks by integrating kinetics, affinity, biological pathways, and transcriptomic and proteomic data when available.
4. Enrichment analyses are performed either with Cytoscape apps or with the Functional Enrichment analysis tool FunRich[30] (www.funrich.org), which displays the results of the analyses in the form of tables and charts. We have used this roadmap to build and analyze the interaction networks of the ECM bioactive fragment

endostatin,[31] the ECM protein procollagen C-proteinase enhancer-1,[32] proteoglycans,[33] a subnetwork of heparin/heparan sulfate interactions regulating angiogenesis in the pericellular matrix,[22] and ECM–parasite interactomes.[15]

11.3 Identification of Biomolecular Interactions by Surface Plasmon Resonance Imaging

SPRi is useful for screening several hundred potential interactions.[34] We have used the Biacore Flexchip system (GE Healthcare) to monitor up to 300 binding events between one analyte injected in buffer flow and recirculated over the array and 70–100 biomolecules spotted in triplicate on a 1 cm^2 gold surface. The protocol used does not require any chemical modification of the proteins or GAGs prior to spotting and relies on their physical adsorption on bare gold.

SPRi assays were performed as described previously.[31,32,35,36] Glycosaminoglycans and proteins were spotted in triplicate at concentrations of 0.06–1 mg mL^{-1} on a bare gold chip (Gold Affinity chip (GE Healthcare) (Figure 11.1A and B) using a non-contact microarraying system (Piezorray,

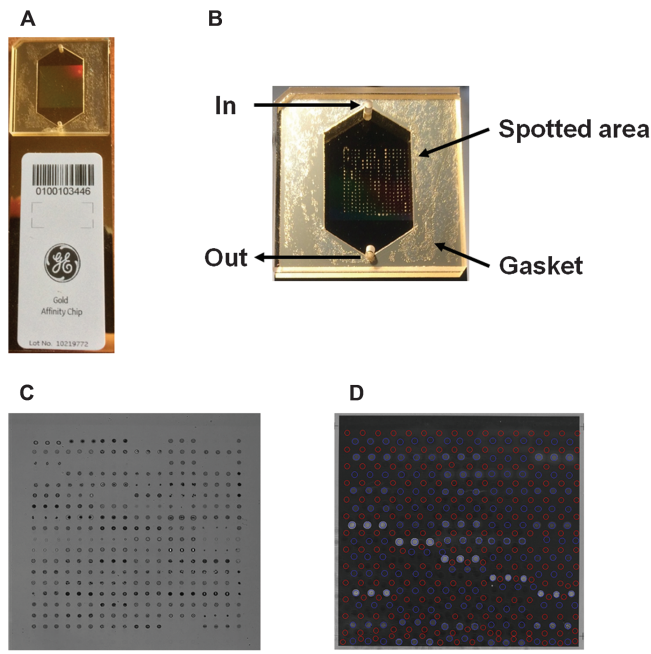

Figure 11.1 (A) Flexchip Gold Affinity chip. (B) Flow cell of the Flexchip Gold Affinity chip (1 cm^2 spotted matrix, 19×18 spots, flow cell volume 46 µL). (C) Flexchip Gold Affinity chip visualized by the CCD camera after spotting. (D) Definition of the regions of interest (spotted biomolecules, blue circles; reference spots, red circles).

PerkinElmer Life Sciences or sciFlexarrayer S3, Scienion) creating a matrix of 225–342 spots (250–300 μm diameter). This non-contact system was selected to avoid damaging the gold-coated plastic grating chip. The spotted chips (Figure 11.1C) were dried and stored under vacuum at 4 °C for 3–4 weeks. The gasket window was sealed over the array to create a unique flow cell of 46 μL (Figure 11.1B). The regions of interest (ROIs), corresponding to the spots of biomolecules, were then defined. Each ROI has four reference spots to correct for bulk refractive index and non-specific binding of the analyte to the surface of the chip (Figure 11.1D).

Tutorial Aspects of SPRi

The Flexchip system does not include a spotting system but several types of arrayers are commercially available. Visual inspection of the spotted arrays is mandatory to check the quality of the spots, which may affect the signal and hence the quality of interaction data.

- The shape of the spots should be regular.
- The spots should be homogeneous.
- The spotted amount should be reproducible.
- The spots should be regularly distributed on the gold surface.

These parameters may be affected by the nature, the molecular weight, and the viscosity of spotted biomolecules, by the buffer used, and by evaporation/drying after spotting.[37]

The experiments were performed at 25 °C. After spotting, the chip surface was blocked five times in a buffer containing mammalian proteins (Biacore Flexchip blocking buffer, GE Healthcare) for 5×5 min and equilibrated with phosphate-buffered saline, 0.05% (v/v) Tween 20 (Sigma) at 500 $\mu L\,min^{-1}$ for 90 min. The analyte was diluted in the same buffer at 500 nM, flowed over the chip surface and recirculated for 20 min at 300–500 $\mu L\,min^{-1}$. The spontaneous dissociation in buffer flow of the complex formed between the spotted ligand and the injected analyte was monitored for 40 min. Data collected from reference spots (bare gold regions and tag spots) were subtracted from those collected on spotted proteins and GAGs to obtain specific binding curves. The chips were used only once because it was difficult to find appropriate conditions to dissociate simultaneously all the complexes formed on the chip surface. Response levels at selected time points were used to rank interactants. In addition, kinetic parameters and equilibrium dissociation constants can be calculated by the Flexchip Evaluation Software 2.1.

The Flexchip system, which has been discontinued by GE Healthcare, had limitations. A single experiment required a large volume of analyte (1.6 mL) and the instrument did not allow the normalization of bulk refractive index

ranks for each signal spot and its four reference spots. In addition, physical adsorption of biomolecules on bare gold may lead to uncontrolled drift in the course of experiments, affecting the kinetics and affinity of interaction (see surface chemistries in Chapter 6). The Flexchip instrument was not designed to perform kinetic titration experiments but it has been successfully used to calculate the kinetics and affinity of antigen–antibody interactions.[34,38,39] However, it is really appropriate for screening purposes and for the identification of new biomolecular interactions between a single analyte injected over hundreds of ligands (''yes/no'' answer), which are used to build comprehensive protein–protein and protein–GAG interaction networks. Furthermore, it is possible to inject whole cells over the arrays to monitor their binding to spotted ligands, as shown for intact, live parasites.[15]

11.4 Building and Functional Analysis of Protein–Glycosaminoglycan Interaction Networks

We built GAG–protein interaction networks using the interaction data we collected by SPRi in a Biacore Flexchip system and by manual curation of the literature. They were stored in the interaction database MatrixDB that we have developed[23–25] (http://matrixdb.univ-lyon1.fr). MatrixDB is a member of the International Molecular Exchange consortium (IMEx) (www.imexconsortium.org) and follows the curation rules of this consortium. The curation process is performed *via* the curation interface of the IntAct database[26] (www.ebi.ac.uk/intact), which is also a member of the IMEx consortium. To take into account the fact that numerous extracellular proteins such as collagens and laminins are multimeric and to discriminate interaction data obtained with multimers from those obtained with individual, isolated, polypeptide chains, we used the identifiers of the complex portal for multimers[40] (www.ebi.ac.uk/intact/complex) and UniProtKB accession numbers for monomeric proteins and the chains of multimers. We built a global GAG–protein interaction network by querying the MatrixDB database for interactions established by heparin (HP), heparan sulfate (HS), chondroitin sulfate (CS), dermatan sulfate (DS), and hyaluronan (HA) with proteins. No interaction of keratan sulfate was available in the MatrixDB database. The interaction network comprised five GAGs, 135 proteins, and 211 interactions (Figure 11.2).

A number of GAG-binding proteins are able to bind to several GAGs (Figure 11.3), showing that the GAG–protein interaction network is highly connected. Heparin has the highest number of protein partners that specifically bind to it. In contrast, all the DS-binding proteins are able to interact with other GAGs (Figure 11.3). Heparan sulfate also has a very small

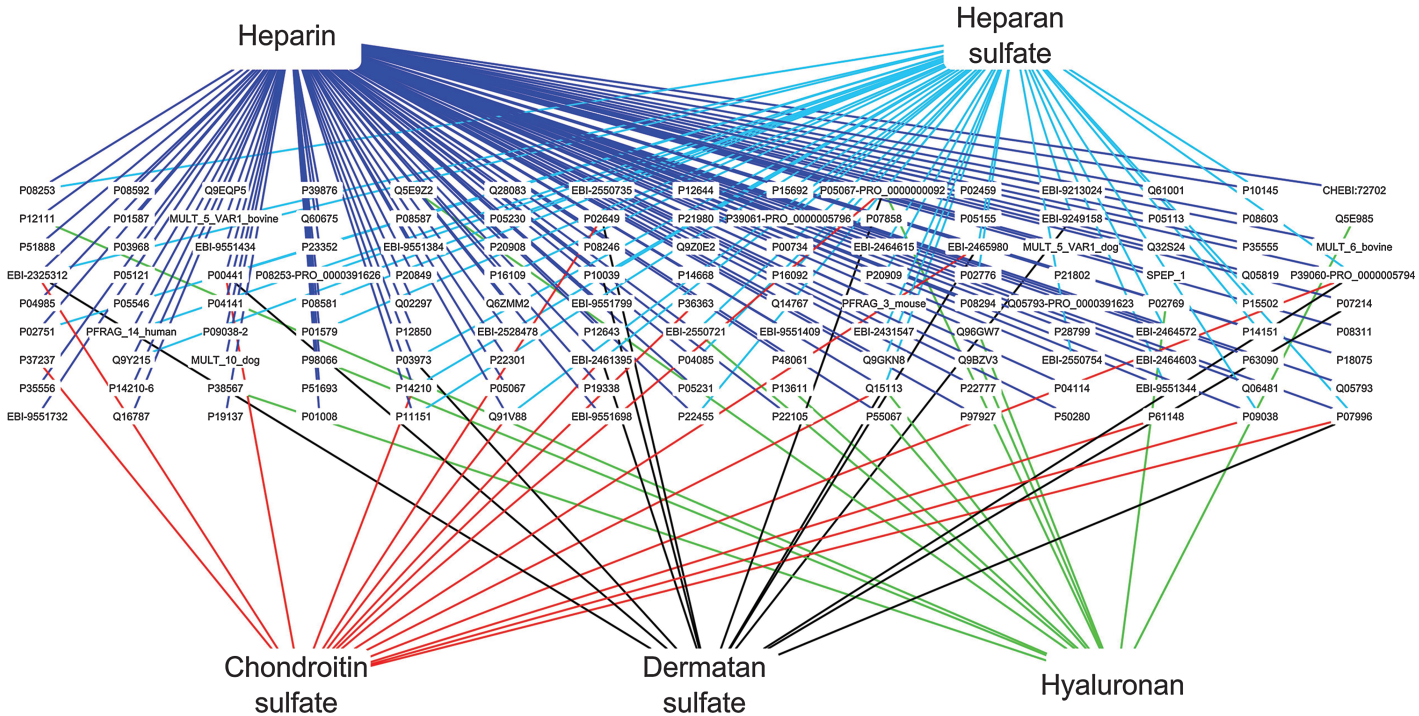

Figure 11.2 Interaction network of the major glycosaminoglycans (CS, DS, HA, HP, and HS) with proteins. Interaction data were collected from MatrixDB[25] and the protein–GAG network was built with Cytoscape.[29] Black, interactions of dermatan sulfate; blue, interactions of heparin; light blue, interactions of heparan sulfate; green, interactions of hyaluronan; red, interactions of chondroitin sulfate. Monomeric proteins are represented by their UniProtKB accession numbers and multimeric proteins by their complex portal identifiers. Bioactive fragments (matricryptins) are labeled by their UniProtKB profeature.

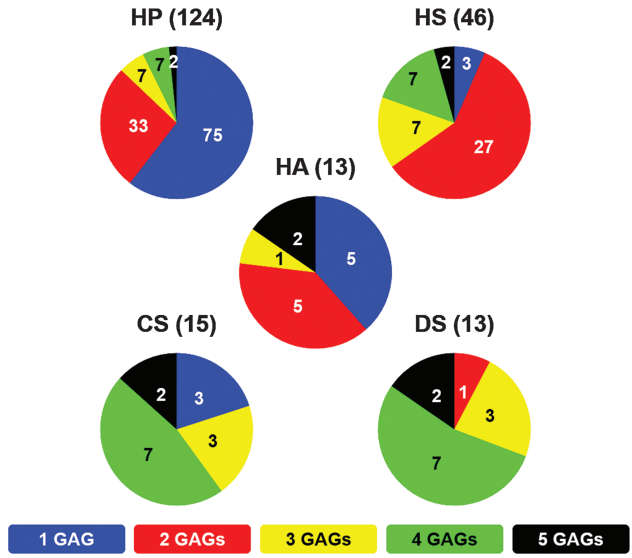

Figure 11.3 The number of proteins interacting with one (blue), two (red), three (yellow), four (green), and five (black) GAGs are indicated for each glycosaminoglycan (HP, heparin; HS, heparan sulfate; CS, chondroitin sulfate; DS, dermatan sulfate; HA, hyaluronan). These data come from the interaction network displayed in Figure 11.2.

number of specific protein partners. This might be because it has the same disaccharide unit as heparin, although the extent and clustering of post-synthetic modifications vary between both GAGs, and also heparin is more widely used than heparan sulfate for interaction studies.

We used the functional enrichment analysis tool FunRich[30] (www.funrich.org) to analyze the GAG–protein interaction network described above. The reference dataset was the human FunRich database.

The enrichment analysis of the term "Cellular component" shows that most GAG-binding proteins are located within the extracellular matrix (Figure 11.4A), which was expected given that GAGs are mostly located within the extracellular matrix and at the cell surface, although some of them have been identified in the nucleus.[41] Seven percent of GAG-binding proteins are located in basement membranes. Regarding "Molecular function," 37% of the GAG-binding proteins are annotated as "extracellular matrix structural constituent," which indicates that they play a role in ECM structural assembly and architecture (Figure 11.4B). In addition, some GAG partners display growth factor activity (7%), cytokine activity (8%), and cell adhesion molecule activity (7%). These functions are significantly enriched over the reference dataset ($p < 0.01$). A total of 39% of GAG-binding partners participate in cell growth and/or maintenance and ~30% in cell communication and signal transduction, but the enrichment in signal

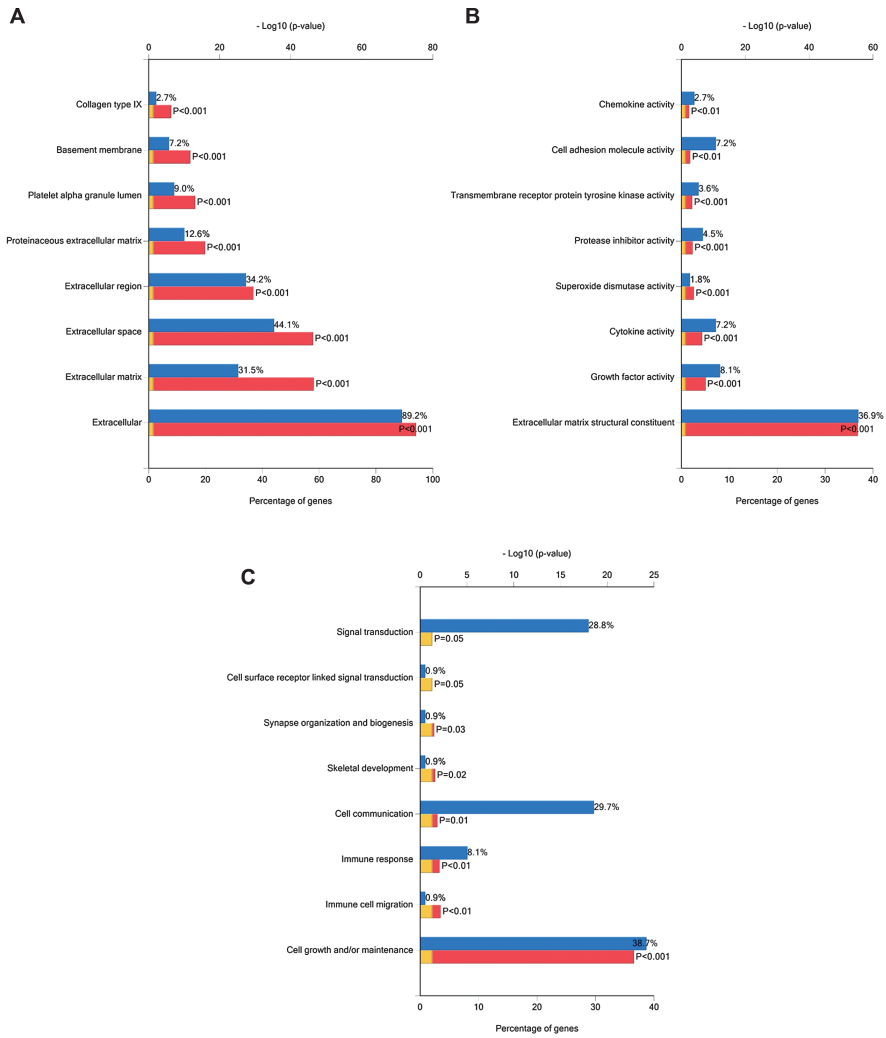

Figure 11.4 Enrichment analyses of the proteins binding to the major glycosaminoglycans (CS, DS, HA, HP, and HS). Interaction data were collected from MatrixDB[25] and enrichment analyses of (A) ''Cellular Component,'' (B) ''Molecular Function,'' and (C) ''Biological Process'' were performed with FunRich.[30] Blue bars, percentage of genes/proteins annotated with a term; red bars, p value; yellow, statistical threshold ($p = 0.05$).

transduction does not reach statistical significance ($p = 0.05$) (Figure 11.4C). In summary GAG-binding proteins identified by querying MatrixDB mostly contribute to the assembly and architecture of the extracellular matrix. In addition to this structural role, one-third of them regulate cell growth and cell communication.

11.5 Contextualization of the Interaction Network with Kinetic Parameters and Affinity

11.5.1 Kinetic and Affinity Data Available in Interaction Databases

These parameters were collected from MatrixDB[25] and from ref. 22. SPR binding assays are widely used to characterize GAG–protein interactions and most values of equilibrium dissociation constants (63%) and association/dissociation rates (60%) stored in the MatrixDB database for heparin/heparan sulfate–protein interactions have been calculated using SPR. Indeed, we used SPR binding assays to characterize the interactions of heparin/heparan sulfate with several ECM proteins, including the matricryptin endostatin,[42] collagens I[43] and V,[43,44] procollagen C-proteinase enhancer-1,[45] angiopoietin like-4,[46] and integrin receptors.[47] For these experiments, biotinylated heparin or heparan sulfate was captured on streptavidin covalently immobilized on CM4 sensor chips and proteins were used as analytes.[43–47]

Kinetic parameters and affinity were used to rank and prioritize interactions within interaction networks. We included only heparin and heparan sulfate in this part of the work because few parameters were available for CS, DS, and HA. Edges of the HP/HS–protein interaction network were color-coded according to the values of the equilibrium dissociation constant (Figure 11.5A) and association rates (Figure 11.5B). The dissociation rates were coded using dots and dashes (Figure 11.5B). Five out of the eight partners of HP and HS bound to both GAGs with similar affinity according to the ranges we defined. The three other partners bound with a higher affinity to HP than to HS (Figure 11.5B). The association rates to HP and HS were in the same range for the three proteins with available data but only one protein dissociated at a similar rate from HP and HS. The two other proteins formed a more stable complex with HP than with HS.

11.5.2 Kinetics and Affinity Calculated by Bio-Layer Interferometry

Bio-Layer Interferometry (BLI) assays were performed to characterize interactions of heparin with three ECM proteins. Collagen I (a triple-helical protein, MW 300 kDa), endostatin, a fragment of collagen XVIII[11,12] (MW 21 kDa), enriched in β-sheets,[48] and the propeptide of the extracellular enzyme lysyl oxidase[49] (MW ~30 kDa) were used as analytes. Collagen I is a rod-like molecule (300 nm in length and 1.5 nm in diameter), the propeptide of lysyl oxidase is intrinsically disordered and thus has an extended conformation, whereas endostatin is a globular protein. The three proteins are basic (p*I* 9.3 for endostatin, 9.6 for collagen I, and 11.8 for the propeptide of lysyl oxidase). Collagen I extracted from human placenta was obtained

from Sigma-Aldrich (C7774). Human endostatin[31] and the propeptide of human lysyl oxidase were both expressed as recombinant proteins in human embryonic kidney cells with the octapeptide FLAG (DYKDDDDK) at their N-terminus and C-terminus, respectively. Both recombinant proteins were expressed and purified in the laboratory by affinity chromatography (Anti-FLAG M2 Agarose; Sigma-Aldrich, A2220).

BLI binding assays were performed with the Octet RED96 (Pall FortéBio) in black 96-well plates at 25 °C in a working volume of 200 µL under orbital agitation at 1000 rpm. This system is described in detail in Chapter 10. Biotinylated heparin was captured *via* streptavidin covalently immobilized

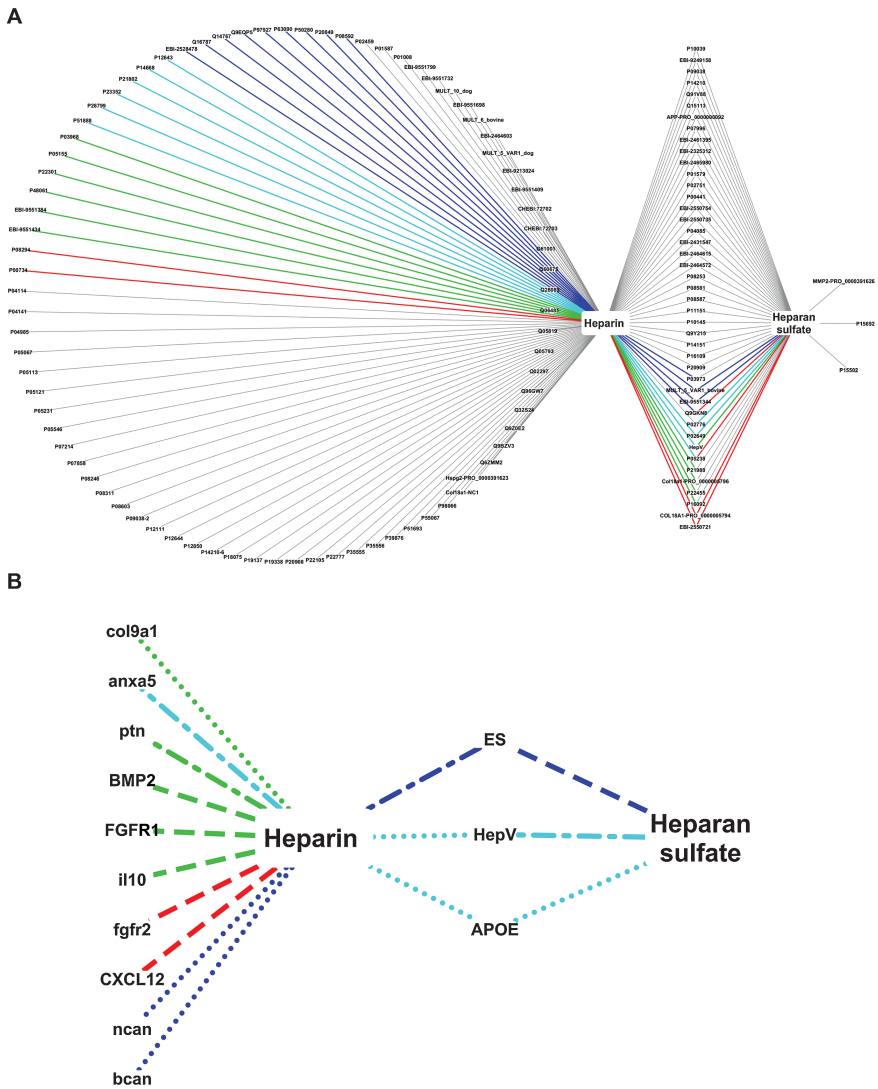

on different streptavidin sensors coated with a proprietary polymer. Prior to each assay, tips were prewetted in 200 μL of HEPES-buffered saline (HBS) for at least 10 min. Streptavidin (SA; designed for immobilization of biotinylated proteins >1 kDa for protein–protein interaction), High Precision Streptavidin (SAX; designed for drug discovery and quality control), and Super Streptavidin (SSA; designed for immobilization of proteins, peptides, and nucleic acids and for small-molecule interactions) sensors were equilibrated in HBS, loaded with 10 or 100 $\mu g\,mL^{-1}$ biotinylated heparin (Sigma-Aldrich, H3393, 16 kDa)[42] in HBS, washed in HBS and equilibrated in HBS-P^+ (endostatin and propeptide of lysyl oxidase) or HBS (collagen I). Binding curves were analyzed using the FortéBio Data Analysis 9.0 software, with a global 1 : 1 model fitting set.

The equilibrium dissociation constant of collagen I–heparin interaction displayed a 1.4-fold increase when calculated from BLI experiments performed on an SA sensor compared with the value determined by SPR experiments carried out on a CM4 sensor chip, but both values are in the low nanomolar range (4.8 nM by BLI *versus* 3.4 nM by SPR[43]) (Table 11.1). The equilibrium dissociation constant of the endostatin–heparin interaction varied by 1.5-fold when calculated from data collected on SSA, which allows a high immobilization density, and SAX sensors. Both the association and dissociation rates were decreased by 2.3- and 1.7-fold, respectively, on an SSA sensor compared with an SAX sensor, but the measurements performed on the SAX sensor had a large standard deviation (Table 11.1). The nature of the sensor surface coating influences the value of the equilibrium dissociation constant and of the kinetic parameters of HP–endostatin interactions.

We then investigated the binding of the propeptide of lysyl oxidase to heparin using an SSA sensor (Figure 11.6). The curves displayed negative shifts and were flipped to calculate kinetic parameters and affinity. Flipping of the data can be performed because the responses were proportional to the analyte concentration, and values of kinetic parameters were validated to be

Figure 11.5 Heparin/heparan sulfate–protein interaction networks contain 124 and 46 proteins, respectively, and share 43 partners. Proteins binding to both GAGs are displayed in the center. (A) Edges connecting GAGs and GAG-binding proteins were color-coded according to the value of the equilibrium dissociation constants (K_D). Gray, no data available; blue, 0.3–10 nM; cyan, 10.5–20 nM; green, 36–400 nM; red, 1140–10 000 nM. (B) Edges connecting GAGs and GAG-binding proteins were color-coded according to the value of the association rate (blue, 2.23–9.04×10^3 $M^{-1}s^{-1}$; cyan, 1.9–7.6×10^4 $M^{-1}s^{-1}$; green, 1.4–6.6×10^5 $M^{-1}s^{-1}$; red, 2.1–2.16×10^6 $M^{-1}s^{-1}$). For the dissociation rate the code was the following: dotted, 2.3–6.6×10^{-4} s^{-1}; dashed-dotted, 1.2–4.3×10^{-3} s^{-1}; dashed, 1–8.3×10^{-2} s^{-1}). Kinetic and affinity data were extracted from MatrixDB database.[25] The interaction network was built with Cytoscape.[29] Monomeric proteins were labeled according to their gene name. Multimeric proteins were labeled with their Complex Portal identifiers and bioactive fragments (matricryptins) by their UniProtKB profeature. ES, endostatin; HepV, a fragment of the collagen α_1(V) chain.

Table 11.1 Kinetic parameters and equilibrium dissociation constant of heparin–protein interaction calculated from BLI experiments performed in HBS-P^+ with Super Streptavidin (SSA) or High Precision Streptavidin (SAX) sensors or in HBS with streptavidin (SA) sensors for collagen I. Collagen I, 0.26–67 nM; endostatin, 0.16–10 μM; propeptide of lysyl oxidase, 0.22–14 μM. Data were fitted to a 1 : 1 model.

Collagen I	SA	
Association rate ($M^{-1}\,s^{-1}$)	$2.8 \pm 0.6 \times 10^5$	
Dissociation rate (s^{-1})	$1.3 \pm 0.5 \times 10^{-3}$	
K_D (nM)	4.8 ± 2.9	
Endostatin	**SSA**	**SAX**
Association rate ($M^{-1}\,s^{-1}$)	3.0×10^3	$7.0 \pm 5.2 \times 10^3$
Dissociation rate (s^{-1})	9.8×10^{-5}	$1.7 \pm 1.6 \times 10^{-4}$
K_D (nM)	31.8	21.3 ± 7.2
Propeptide of lysyl oxidase	**SSA (HP 16 kDa)**	**SSA (HP 6 kDa)**
Association rate ($M^{-1}\,s^{-1}$)	2.1×10^2	1.9×10^2
Dissociation rate (s^{-1})	2.1×10^{-4}	3.6×10^{-5}
K_D	1.0 μM	190 nM

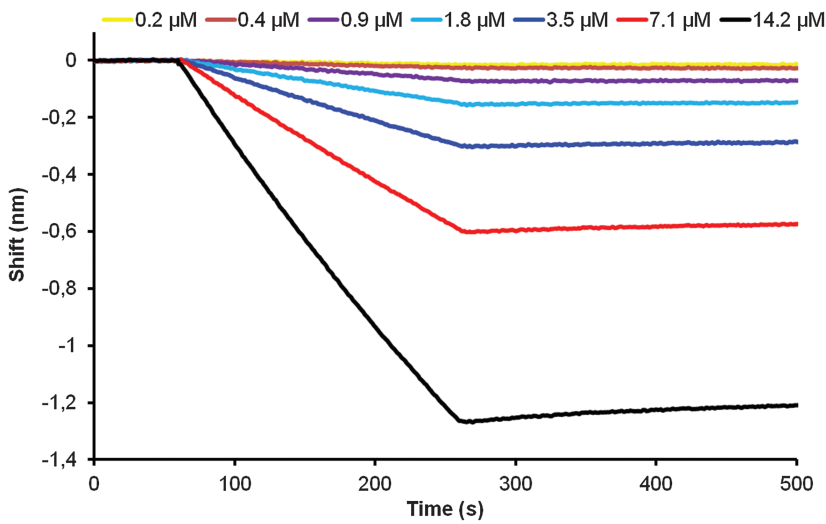

Figure 11.6 Bio-Layer Interferometry analyses of the binding of the propeptide of lysyl oxidase (0.2–14.2 μM) to heparin from porcine intestinal mucosa (H3393) biotinylated as described[42] and captured on an SSA sensor. The data were flipped as described in ref. 50.

independent of the magnitude of the nm shift.[50] A negative signal can occur when the optical thickness decreases upon binding. This can be due either to the release of a cofactor or when a more closely packed structure is obtained by a conformational change of the ligand.

Last, we determined the influence of heparin size (6 and 16 kDa) on kinetics and affinity calculated for the heparin-LOX propeptide on a SSA sensor. The propeptide bound to both heparins at a similar rate but dissociated faster from full-length heparin, leading to a 5-fold decrease in the value of the equilibrium dissociation constant for 6-kDa heparin (Table 11.1). The propeptide bound with a higher affinity to 6-kDa heparin than to 16-kDa heparin.

Tutorial Aspects of BLI (see BLI features and benefits in Chapter 10)

- For accurate measurements, be aware of reflections from the bottom of the well plate causing jumps in the response curves. There are protocols to prevent this (see Chapter 10, Section 10.5.2.2).
- SPR applies a boost of the evanescent field by a factor of ~30 (see Chapter 2, Section 2.3.4) and is intrinsically more sensitive than BLI.
- Why do we need to flip the interaction curves and what is the reason that these negative responses are measured? See answer to question 2 at the end of this book.

11.6 Conclusion

We have set up a roadmap for building and analyzing GAG–protein interaction networks, for integrating kinetics and affinity into these networks, and for analyzing them by performing functional enrichment analyses. Label-free interaction analysis is a crucial tool for calculating the binding strength and kinetics of the interactants in the networks. Screening of potential interacting pairs was performed by SPRi in a Biacore Flexchip system, whereas the association and dissociation rates and the equilibrium dissociation constants were determined by either SPR or BLI. We studied the binding of heparin with three proteins by BLI using three different streptavidin sensors and showed that these surfaces influence the calculated values of equilibrium dissociation constant, and the association and dissociation rates of heparin–protein interactions. These changes are associated at least in part with the conformation, the isoelectric point, and the post-translational modifications (*e.g.* glycosylation) of the proteins and are likely to be protein dependent. The molecular mechanisms underlying the biological functions of the biomolecular interaction networks can be revealed using a combination of instruments based on SPRi, SPR, and BLI and bioinformatic tools as shown in this chapter.

11.7 Abbreviations

BLI Bio-Layer Interferometry
CS chondroitin sulfate

DS	dermatan sulfate
ECM	extracellular matrix
EDC	1-ethyl-3-(3-dimethylaminopropyl) carbodiimide hydrochloride
GAG	glycosaminoglycan
HA	hyaluronan
HBS	HEPES-buffered saline
HEPES	4-(2-hydroxyethyl)-1-piperazineethanesulfonic acid
HP	heparin
HS	heparan sulfate
MW	molecular weight
NHS	*N*-hydroxysulfosuccinimide
RU	resonance unit
SPR	surface plasmon resonance
SPRi	surface plasmon resonance imaging

11.8 Questions

1. The Biacore Flexchip instrument is very useful for identifying protein and glycosaminoglycan partners. Why do we need a combination of instruments based on different approaches (SPRi, SPR, and BLI), as also discussed in Chapter 12, Section 12.2?
2. Why do we need to flip the BLI interaction curves (see Figure 11.6) and what is the reason why negative responses are measured as a result of biomolecular binding?

Acknowledgements

The authors used the SPR and SPRi systems of the Protein Science Facility (UMS 3444/US8, SFR Biosciences, Lyon, France). They thank Loïc Blum and Christophe Marquette (UMR 5246 CNRS, Université Lyon 1, France) and AXO Science (Villeurbanne, France) for access to the spotter. This work was supported in part by a grant from the Fondation pour la Recherche Médicale (DBI20141231336) to S.R.-B. and N.T.-M. and by a grant from the Institut Français de Bioinformatique (ANR-11-INS-0013, Glycomatrix project) to S.R.-B. and N.T.-M.

References

1. C. Frantz, K. M. Stewart and V. M. Weaver, *J. Cell Sci.*, 2010, **123**, 4195–4200.
2. A. D. Theocharis, S. S. Skandalis, C. Gialeli and N. K. Karamanos, *Adv. Drug Delivery Rev.*, 2016, **97**, 4–27.
3. M. A. Karsdal *et al.*, *Assay Drug Dev. Technol.*, 2013, **11**, 70–92.
4. P. Lu, K. Takai, V. M. Weaver and Z. Werb, *Cold Spring Harbor Perspect. Biol.*, 2011, **3**, a005058.

5. T. R. Cox and J. T. Erler, *Dis. Models & Mech.*, 2011, **4**, 165–178.
6. B. N. Brown and S. F. Badylak, *Transl. Res. J. Lab. Clin. Med.*, 2014, **163**, 268–285.
7. H. Järveläinen, A. Sainio, M. Koulu, T. N. Wight and R. Penttinen, *Pharmacol. Rev.*, 2009, **61**, 198–223.
8. R. O. Hynes and A. Naba, *Cold Spring Harbor Perspect. Biol.*, 2012, **4**, a004903.
9. A. Naba, K. R. Clauser, H. Ding, C. A. Whittaker, S. A. Carr and R. O. Hynes, *Matrix Biol.*, 2016, **49**, 10–24.
10. S. Ricard-Blum and R. Salza, *Exp. Dermatol.*, 2014, **23**, 457–463.
11. S. Ricard-Blum and S. D. Vallet, *Biochimie*, 2016, **122**, 300–313.
12. S. Ricard-Blum and S. D. Vallet, *Front. Pharmacol.*, 2016, **7**, 11.
13. A. Walia *et al.*, *Biochim. Biophys. Acta*, 2015, **1850**, 2422–2438.
14. S. Wang, X.-A. Lu, P. Liu, Y. Fu, L. Jia, S. Zhan and Y. Luo, *Mol. Cancer Ther.*, 2015, **14**, 1192–1201.
15. M. Fatoux-Ardore, F. Peysselon, A. Weiss, P. Bastien, F. Pratlong and S. Ricard-Blum, *Infect. Immun.*, 2014, **82**, 594–606.
16. R. V. Iozzo and L. Schaefer, *Matrix Biol.*, 2015, **42**, 11–55.
17. J.-P. Li and M. Kusche-Gullberg, *Int. Rev. Cell Mol. Biol.*, 2016, **325**, 215–273.
18. J. D. Esko and S. B. Selleck, *Annu. Rev. Biochem.*, 2002, **71**, 435–471.
19. R. Sasisekharan, Z. Shriver, G. Venkataraman and U. Narayanasami, *Nat. Rev. Cancer*, 2002, **2**, 521–528.
20. A. Ori, M. C. Wilkinson and D. G. Fernig, *J. Biol. Chem.*, 2011, **286**, 19892–19904.
21. D. Xu and J. D. Esko, *Annu. Rev. Biochem.*, 2014, **83**, 129–157.
22. F. Peysselon and S. Ricard-Blum, *Matrix Biol.*, 2014, **35**, 73–81.
23. E. Chautard, L. Ballut, N. Thierry-Mieg and S. Ricard-Blum, *Bioinformatics*, 2009, **25**, 690–691.
24. E. Chautard, M. Fatoux-Ardore, L. Ballut, N. Thierry-Mieg and S. Ricard-Blum, *Nucleic Acids Res.*, 2011, **39**, D235–D240.
25. G. Launay, R. Salza, D. Multedo, N. Thierry-Mieg and S. Ricard-Blum, *Nucleic Acids Res.*, 2015, **43**, D321–D327.
26. S. Orchard *et al.*, *Nat. Methods*, 2012, **9**, 345–350.
27. S. Orchard *et al.*, *Nucleic Acids Res.*, 2014, **42**, D358–D363.
28. J. M. Brockman and S. M. Fernandes, *Am. Lab.*, 2001, **33**, 37–41.
29. P. Shannon *et al.*, *Genome Res.*, 2003, **13**, 2498–2504.
30. M. Pathan *et al.*, *Proteomics*, 2015, **15**, 2597–2601.
31. C. Faye, E. Chautard, B. R. Olsen and S. Ricard-Blum, *J. Biol. Chem.*, 2009, **284**, 22041–22047.
32. R. Salza *et al.*, *Biochem. J.*, 2014, **457**, 137–149.
33. F. Peysselon, M. Fatoux-Ardore and S. Ricard-Blum, in *From Binary Interactions of Glycosaminoglycans and Proteoglycans to Interaction Networks*, Matrix Biology Institute, Edgewater, New Jersey, USA, ed. Endre A. Balazs, 2012, **5**, 277–298.
34. R. L. Rich *et al.*, *Anal. Biochem.*, 2008, **373**, 112–120.

35. S. Symoens *et al.*, *Biochem. J.*, 2011, **433**, 371–381.
36. C. Bonod-Bidaud *et al.*, *J. Invest. Dermatol.*, 2012, **132**, 1841–1849.
37. R. Wellhausen and H. Seitz, *J. Biomed. Biotechnol.*, 2012, **2012**, 831347.
38. D. Wassaf *et al.*, *Anal. Biochem.*, 2006, **351**, 241–253.
39. R. L. Rich *et al.*, *Anal. Biochem.*, 2009, **386**, 194–216.
40. B. H. M. Meldal *et al.*, *Nucleic Acids Res.*, 2015, **43**, D479–D484.
41. M. D. Stewart and R. D. Sanderson, *Matrix Biol.*, 2014, **35**, 56–59.
42. S. Ricard-Blum *et al.*, *J. Biol. Chem.*, 2004, **279**, 2927–2936.
43. S. Ricard-Blum, M. Beraud, N. Raynal, R. W. Farndale and F. Ruggiero, *J. Biol. Chem.*, 2006, **281**, 25195–25204.
44. S. Ricard-Blum, L. L. Peel, F. Ruggiero and N. J. Freeman, *Anal. Biochem.*, 2006, **352**, 252–259.
45. T. Weiss, S. Ricard-Blum, L. Moschcovich, E. Wineman, S. Mesilaty and E. Kessler, *J. Biol. Chem.*, 2010, **285**, 33867–33874.
46. C. Chomel, A. Cazes, C. Faye, M. Bignon, E. Gomez, C. Ardidie-Robouant, A. Barret, S. Ricard-Blum, L. Muller, S. Germain and C. Monnot, *FASEB J.*, 2009, **23**, 940–949.
47. C. Faye, C. Moreau, E. Chautard, R. Jetne, N. Fukai, F. Ruggiero, M. J. Humphries, B. R. Olsen and S. Ricard-Blum, *J. Biol. Chem.*, 2009, **284**, 22029–22040.
48. Y. H. Ding, K. Javaherian, K. M. Lo, R. Chopra, T. Boehm, J. Lanciotti, B. A. Harris, Y. Li, R. Shapiro, E. Hohenester, R. Timpl, J. Folkman and D. C. Wiley, *Proc. Natl. Acad. Sci. U. S. A.*, 1998, **95**, 10443–10448.
49. S. R. Vora, Y. Guo, D. N. Stephens, E. Salih, E. D. Vu, K. H. Kirsch, G. E. Sonenshein and P. C. Trackman, *Biochemistry*, 2010, **49**, 2962–2972.
50. B. Heidecker, K. Witte and W. McGinn-Straub, *Octet Appl. Note*, 2011, **3**, 1–8.